Different transport routes for high density lipoprotein and its associated free sterol in polarized hepatic cells[S]

Daniel Wüstner,[1] Mousumi Mondal, Amy Huang, and Frederick R. Maxfield[2]

Department of Biochemistry, Weill Medical College of Cornell University, New York, NY 10021

Abstract **We analyzed the intracellular transport of HDL and its associated free sterol in polarized human hepatoma HepG2 cells. Using pulse-chase protocols, we demonstrated that HDL labeled with Alexa 488 at the apolipoprotein (Alexa 488-HDL) was internalized by a scavenger receptor class B type I (SR-BI)-dependent process at the basolateral membrane and became enriched in a subapical/apical recycling compartment. Most Alexa 488-HDL was rapidly recycled to the basolateral cell surface and released from cells. Within 30 min of chase at 37°C, ~3% of the initial cell-associated Alexa 488-HDL accumulated in the biliary canaliculus (BC) formed at the apical pole of polarized HepG2 cells. Even less Alexa 488-HDL was transported to late endosomes or lysosomes. The fluorescent cholesterol analog dehydroergosterol (DHE) incorporated into Alexa 488-HDL was delivered to the BC within a few minutes, independent of the labeled apolipoprotein. This transport did not require metabolic energy and could be blocked by antibodies against SR-BI. The fraction of cell-associated DHE transported to the BC was comparable when cells were incubated with either Alexa 488-HDL containing DHE or with DHE bound to methyl-β-cyclodextrin. We conclude that rapid, nonvesicular transport of sterol to the BC and efficient recycling of HDL particles underlies the selective sorting of sterol from HDLs in hepatocytes.**—Wüstner, D., M. Mondal, A. Huang, and F. R. Maxfield. **Different transport routes for high density lipoprotein and its associated free sterol in polarized hepatic cells.** ***J. Lipid Res.*** **2004.** 45: **427–437.**

Supplementary key words hepatocytes • dehydroergosterol • bile • fluorescence microscopy

During reverse cholesterol transport, HDLs deliver free cholesterol and cholesteryl ester from peripheral tissues to the liver (1). This sterol can be used for the synthesis of bile salts, incorporated into VLDLs for secretion, or released into the bile at the apical (canalicular) membrane of hepatocytes. Biliary secretion of cholesterol and bile salts is the only pathway of sterol clearance from the body (1). However, the mechanisms underlying the continuous transport of lipids and proteins into the biliary canaliculus (BC) remain to be fully determined. Several lines of evidence suggest that the intracellular fate of esterified cholesterol is different from that of free cholesterol derived from HDL. Using various lipoproteins labeled with plant sterols, Robins and Fasulo (2) demonstrated that HDL, but no other lipoproteins, provide a vehicle for sterol transport to bile. By perfusion of rat livers with HDL containing the plant sterol sitostanol, it was shown that sitostanol was secreted into the bile within 2–4 min after adding the lipoprotein to the perfusate (3). It was concluded that the unesterified sterol was delivered by a plasma membrane pathway independent of the uptake of HDL. Release of cholesterol from the canalicular membrane into the bile is probably mediated by the ATP binding cassette (ABC) half-transporters ABCG5 and ABCG8 (4, 5).

There have been several studies of the uptake and intracellular transport of HDL in hepatocytic cells. Several studies have characterized a retroendocytic pathway for HDL in hepatocytes and hepatoma HepG2 cells by which internalized HDL has been proposed to recycle rapidly toward the basolateral membrane surface (6–8). By this process, HDL-associated lipids can be delivered to the hepatocyte (8). HDL was found to colocalize with the recycling marker transferrin (Tf) in an endocytic recycling compartment (ERC) in primary hepatocytes after perfusion with labeled HDL (9). This enrichment in an ERC was reduced in ob/ob hepatocytes, which also had defects in up-

Abbreviations: Alexa 488-HDL, Alexa 488-labeled high density lipoprotein; apoA-I, apolipoprotein A-I; BC, biliary canaliculus; DHE, dehydroergosterol; DHE/Alexa 488-HDL, Alexa 488-labeled high density lipoprotein containing dehydroergosterol; DHE/MβCD, DHE loaded on methyl-β-cyclodextrin; DiI-C18 dioctadecanoyl-3,3,3′,3′-tetramethylindocarbocyanine perchlorate; ERC, endocytic recycling compartment; MβCD, methyl-β-cyclodextrin; PC, phosphatidylcholine; PFA, paraformaldehyde; ROI, region of interest; SAC/ARC, subapical compartment/apical recycling compartment; SR-BI, scavenger receptor class B type I; Tf, transferrin.

[1] Present address of D. Wüstner: Theoretical Biophysics Group, Max-Delbrück-Center for Molecular Medicine, Robert-Rössle Str. 10, 13125, Berlin, Germany.

[2] To whom correspondence should be addressed.
e-mail: frmaxfie@med.cornell.edu

[S] The online version of this article (available at http://www.jlr.org) contains an additional two figures.

Manuscript received 24 October 2003.

Published, JLR Papers in Press, December 16, 2003.
DOI 10.1194/jlr.M300440-JLR200

take of HDL and lipids associated with the particle. It was concluded that HDL recycling through the ERC might play an important role in the determination of plasma HDL protein and cholesterol levels.

Using the naturally fluorescent cholesterol analog dehydroergosterol (DHE), we studied sterol transport in polarized human hepatoma HepG2 cells. Those cells form an apical vacuole closely resembling the BC of hepatocytes (10). By selectively incorporating DHE into the plasma membrane of HepG2 cells using DHE bound to methyl-β-cyclodextrin (DHE/MβCD), we demonstrated that this sterol becomes enriched in a subapical compartment/apical recycling compartment (SAC/ARC) but did not accumulate in the *trans*-Golgi network (11). In contrast to fluorescent phosphatidylcholine (PC), which traversed HepG2 cells in vesicles in both directions via the SAC/ARC, once DHE became associated with SAC/ARC membranes it did not redistribute to a great extent to either plasma membrane domain (11, 12). For DHE and fluorescent PC, we demonstrated that a rapid, nonvesicular, and largely ATP-independent transport pathway delivers these lipids to the canalicular membrane of HepG2 cells. This pathway might be controlled, in part, by the rate of transbilayer migration of those lipids across the plasma membrane of the cells.

To further understand the fate of HDL and its associated sterol in hepatic cells requires an analysis of the intracellular trafficking of HDL and of sterol incorporated into HDL particles. Using quantitative fluorescence microscopy and image analysis, we show in this paper that HDL is internalized into the same vesicles as Tf and is transported to a SAC/ARC in polarized HepG2 cells. Whereas more than 50% of Alexa 488-labeled HDL (Alexa 488-HDL) recycles to the basolateral membrane, some Alexa 488-HDL accumulated in the BC with a time course suggestive of transit through the SAC/ARC. Enrichment of DHE derived from HDL into the BC preceded the arrival of the fluorescently labeled apolipoprotein. ATP depletion completely blocked the uptake of fluorescent apolipoprotein particles by HepG2 cells but not the uptake and transport of HDL-derived DHE to the BC. These results suggest that nonvesicular transport delivers DHE selectively to the canalicular membrane. Uptake of Alexa 488-HDL as well as nonvesicular shuttling of DHE to the canalicular membrane could be partly blocked by antibodies against scavenger receptor class B type I (SR-BI). The relevance of these results for the mechanisms underlying reverse cholesterol transport and biliary lipid secretion are discussed.

EXPERIMENTAL PROCEDURES

Reagents

Succinimidyl esters of Alexa 488, Alexa 546, and Alexa 633 were purchased from Molecular Probes, Inc. (Eugene, OR). Medium 1 contained 150 mM NaCl, 5 mM KCl, 1 mM $CaCl_2$, 1 mM $MgCl_2$, 5 mM glucose, and 20 mM HEPES (pH 7.4). Medium 2 was identical to medium 1 except that it contained no glucose but 5 mM sodium azide and 50 mM 2-deoxyglucose for energy depletion of cells (see below). Release medium is medium 1 supplemented with 25.5 mM citric acid, 24.5 mM sodium citrate, and 100 mM deferoxamine mesylate, adjusted to pH 5.2, and containing 280 mM sucrose instead of glucose (see above). Rhodamine-labeled dextran (70 kDa) was dissolved in PBS and repeatedly dialyzed before use to remove unconjugated dye. FCS and DMEM were from GIBCO BRL (Life Technologies, Paisley, UK). All other chemicals were from Sigma Chemical Co. (St. Louis, MO). Tf was iron loaded as previously described (13). Succinimidyl esters of Alexa 546 were then conjugated to the iron-loaded Tf according to the manufacturer's instructions. Human apolipoprotein A-I (apoA-I) was obtained from Biodesign (Saco, ME). Human HDL_3 was kindly provided by Drs. David Silver and Ira Tabas (Columbia University, New York, NY). It was labeled with Alexa 488 according to the manufacturer's instructions. Alexa 488-labeled HDL (Alexa 488-HDL) was purified by gel filtration on a Sephadex B column and dialyzed three times against PBS at 4°C overnight. Antibodies to SR-BI (14) were provided by Drs. David Silver and Alan Tall (Columbia University). Asialo-orosomucoid (ASOR) was provided by Drs. Allan Wolkoff and Richard Stockert (Albert Einstein College of Medicine, New York, NY) and was labeled with the succinimidyl ester of Alexa 633 according to the manufacturer's instructions.

Cell culture

HepG2 cells were grown in DMEM with 4.5 g/l glucose supplemented with 10% heat-inactivated FCS and antibiotics. Cells were routinely passaged in plastic tissue culture dishes. For experiments, cells were plated onto glass coverslips coated with poly-D-lysine and used after reaching the highest degree of polarization as described previously (12).

Preparation of lipid solutions and of Alexa 488-HDL labeled with DHE

DHE/cyclodextrin complexes. A stock solution of DHE (5 mM) was made in ethanol and stored under argon. For labeling of cells with DHE, the analog was loaded on MβCD as described previously (11, 15). The final MβCD-DHE ratio was 1:8 (mol/mol) (16).

DHE-labeled Alexa 488-HDL. Alexa 488-HDL was labeled with DHE by incubating the lipoprotein with DHE/MβCD at 37°C. The transfer kinetics and efficiency of DHE were measured online at λex = 326 nm and λem = 370 nm on a Spex Fluorolog spectrofluorometer (Spex Industries, Inc., Edison, NJ). This is based on an increase of the fluorescence monomer peak of DHE upon addition of HDL to the DHE/MβCD solution attributable to the incorporation of DHE as monomers into the phospholipid monolayer of the lipoprotein particle. DHE-labeled Alexa 488-HDL (DHE/Alexa 488-HDL) was purified by gel filtration on a Sephadex B column. Fractions with the highest ratios of Alexa 488 to DHE fluorescence measured at λex = 480 and 326 nm, respectively, were collected and dialyzed against medium 1 at 4°C overnight. The degree of purification was tested by recording DHE excitation and emission spectra in purified DHE/Alexa 488-HDL solutions, which were then compared with DHE membrane spectra in liposomes. Excitation and emission spectra of purified DHE/Alexa 488-HDL showed all of the characteristics of membrane spectra of DHE, and no remaining peak of the blue-shifted emission maxima for DHE bound to MβCD could be detected (data not shown) (11, 17). Thus, complete removal of MβCD from the labeled lipoprotein was concluded. Fluorescence properties of DHE incorporated into Alexa 488-HDL were not altered by the presence of the Alexa 488 fluorophore.

Uptake and transport of Alexa 488-HDL in polarized and nonpolarized HepG2 cells

Colocalization with Alexa 546-Tf. Cells were colabeled with 2 μg/ml Alexa 488-HDL and with 10 μg/ml Alexa 546-Tf for 1 or 10 min at 37°C, washed, and chased at 37°C in medium 1 for the indicated time periods (see Fig. 3). These experiments were performed in control and in ATP-depleted cells (see below) with medium 2 being the chase medium for ATP-depleted cells.

Colocalization with rhodamine-dextran and Alexa 633-labeled ASOR. To load the lysosomal pathway, cells were labeled with 2.5 mg/ml rhodamine-dextran for 1 h at 37°C. They were washed and pulse-labeled with 2 μg/ml Alexa 488-HDL for either 1 or 10 min at 37°C. In some experiments, cells were also incubated with Alexa 633-labeled ASOR (Alexa 633-ASOR) to label endosomes and lysosomes. After incubations, cells were washed and imaged on a wide-field microscope as described below.

Competition experiments and energy depletion. To test saturable uptake of HDL, HepG2 cells were labeled with 2 μg/ml Alexa 488-HDL in the presence of a 40-fold excess of unlabeled HDL for 2 min at 37°C (see Fig. 1). Those cells were washed and imaged, and the fluorescence intensity of Alexa 488-HDL in the cells was quantified as described below. To determine if uptake was mediated by SR-BI, cells were incubated with an SR-BI antibody for 10 min before the addition of labeled HDL. Alternatively, cells were incubated in the presence of excess (40 μg/ml) unlabeled, lipid-free apoA-I. For energy depletion, cells were incubated for 30 min at 37°C in medium 2 containing 5 mM sodium azide and 50 mM 2-deoxyglucose. In those experiments designed to determine the energy dependence of transport processes, all further incubation steps except labeling with DHE/MβCD or DHE/Alexa 488-HDL and rhodamine-dextran were performed in medium 2. Uptake of Alexa 546-Tf was tested as previously described after a mild acid wash with release medium to remove surface-bound Alexa 546-Tf (11). Additionally, ATP-depleted cells were double labeled with Alexa 546-Tf and Alexa 488-HDL, washed with medium 2, and fixed with paraformaldehyde (PFA). Those cells were imaged by acquiring stacks in the green and red channel to visualize any intracellular fluorescence of the probes as described below.

Intracellular transport of DHE derived from Alexa 488-HDL or from DHE/MβCD. Cells were labeled with 2.5 mg/ml rhodamine-dextran for 1 h, washed, and labeled for 1 min at 37°C with either DHE/Alexa 488-HDL or DHE/MβCD. Those cells were washed and immediately imaged on a wide-field microscope. This experiment was performed in control and ATP-depleted cells (see above). Alternatively, cells were chased for various times at 37°C before imaging (see Results). In some experiments, cells were preincubated with antibodies against SR-BI for 5 min at 37°C and labeled with DHE/Alexa 488-HDL for 10 min at 37°C in the presence of the SR-BI antibody.

Fluorescence microscopy and image analysis. Wide-field fluorescence microscopy and digital image acquisition were routinely carried out using a Leica DMIRB microscope with a 63×, 1.4 numerical aperture oil-immersion objective (Leica Lasertechnik GmbH, Wetzlar, Germany) equipped with a Princeton Instruments cooled charge-coupled device camera driven by Image-1/MetaMorph Imaging System software (Universal Imaging Inc.). Rhodamine-dextran and Alexa 546-Tf were imaged using a standard rhodamine filter set [535 nm (50 nm band-pass) excitation filter, 565 nm long-pass dichromatic filter, and 610 nm (75 nm band-pass) emission filter], and Alexa 488-HDL was imaged using a standard fluorescein filter set [470 nm (20 nm band-pass) excitation filter, 510 nm long-pass dichromatic filter, and 537 nm (23-nm band-pass) emission filter]. DHE was imaged using a specially designed filter cube obtained from Chroma Technology Corp. (Brattleboro, VT) with 335 nm (20 nm band-pass) excitation filter, 365 nm long-pass dichromatic filter, and 405 nm (40 nm band-pass) emission filter as described previously (18). Alexa 633 was imaged with a 640 nm (20 nm band-pass) exciter, a 660 nm dichromatic filter, and a 680 nm (30 nm band-pass) emission filter set. All other components of the microscope were adapted for ultraviolet imaging as described previously (15). Image analysis was carried out using Image-1/MetaMorph Imaging System software. Determination and subtraction of crossover of fluorescence between the channels was performed as described (19, 20).

Quantitative assessment of trafficking of Alexa 488-HDL and DHE. To assess the competitive uptake of labeled HDL, images were corrected for off-cell background intensity. The total fluorescence power above a threshold intensity per pixel was determined for the entire image. This fluorescence power was then normalized by dividing by the number of cells in the field. In polarized HepG2 cells stained with Alexa 488-HDL and colabeled with rhodamine-dextran or Alexa 546-Tf, fluorescence in the SAC/ARC and BC was quantified by defining regions of interest (ROIs) for these compartments based on the fluorescence of rhodamine-dextran (for the BC) or of Alexa 546-Tf (for the SAC/ARC). To quantify the fluorescence of DHE derived from DHE/MβCD in the SAC/ARC, this compartment was identified by defining a subapical region in the cells containing more than 80% of DHE fluorescence above cellular background levels from the last image of a time series (see Results). This region was next used as a mask for the quantification of DHE fluorescence in the SAC/ARC for all time points. To assess the effect of antibodies against SR-BI on the uptake of DHE, cells preincubated with the antibody were labeled for 10 min at 37°C in the presence of DHE/Alexa 488-HDL and SR-BI antibody. Fluorescence of DHE was measured as average intensity per pixel for all cells outlined from the corresponding differential interference contrast image. Intensities corrected for background fluorescence were averaged from six fields for each condition.

Fluorescence intensity in all ROIs was measured after background subtraction and normalized to total cell-associated fluorescence of Alexa 488-HDL or DHE in the two cells forming a BC. The ratio R(t) of the integrated fluorescence intensity of ROI [$I_{ROI}(t)$] and of whole cells [$I_{cell}(t)$] was then calculated and plotted as function of time (see Fig. 4):

$$R(t) = \frac{I_{ROI}(t)}{I_{cell}(t)} \qquad \textit{(Eq. 1)}$$

Similarly, the fluorescence of DHE derived from Alexa 488-HDL or from cyclodextrin was quantified for the BC based on the fluorescence of rhodamine-dextran and for cells forming a BC (11).

To determine the fraction of Alexa 488-HDL transported along the lysosomal pathway, late endosomes and lysosomes were identified by the fluorescence of rhodamine-dextran. To this end, a mask was generated for the rhodamine image by applying a threshold that accounts for 20% of the brightest fluorescence of rhodamine-dextran in the BC to the whole field (21, 22). This procedure ensured that a large and constant fraction of all rhodamine-labeled endosomes was included despite slight differences in the uptake of rhodamine-dextran by the cells. This mask was applied to the background-corrected image of Alexa 488-HDL. Fluorescence of Alexa 488-HDL in rhodamine-dextran-containing endosomes but not that in the BC was measured and normalized to total cell-associated fluorescence of Alexa 488-HDL according to equation 1. All measured fluorescence intensities were exported to an Excel spreadsheet (Microsoft, Inc.). For quantification of Alexa 488-HDL in the various compartments as well as for measuring DHE in the BC, the data for four

to six fields with two to three cells forming a BC in each field were averaged, analyzed, and plotted using Sigma Plot 4.0 (SPSS, Inc., Chicago, IL).

To determine the intracellular fluorescence of either Alexa 488-HDL or Alexa 546-Tf, ATP-depleted HepG2 cells (see above) were double labeled with both probes, chased for 30 min in medium 2, and imaged. Using a z-stepper, images were acquired every 0.5 μm through the entire cell in both channels. A sum projection was obtained using MetaMorph software, and intracellular versus plasma membrane fluorescence was compared for both probes.

RESULTS

Analysis of transport of Alexa 488-HDL

We have studied the intracellular transport routes of fluorescently labeled HDL in polarized HepG2 cells. First, we performed competition experiments for the uptake of Alexa 488-HDL by polarized HepG2 cells. As shown in **Fig. 1**, the cellular fluorescence of Alexa 488-HDL could be reduced by ~80% when cells were incubated with a 40-fold excess of unlabeled HDL. Previous studies have shown that the basolateral uptake of HDL is mediated by SR-BI and can be blocked by anti-receptor antibodies (14). Anti-SR-BI antibodies also block the cellular uptake of Alexa 488-HDL by HepG2, indicating that internalization of the fluorescent lipoprotein is mediated mainly by SR-BI (14, 23). In line with this conclusion, we found inhibition of uptake also by excess apoA-I, which has been reported to bind to SR-BI, although with lower affinity than lipidated apoA-I or HDL (24).

To visualize the BC and the endosomal membrane system, HepG2 cells were labeled with rhodamine-dextran for 1 h at 37°C (**Fig. 2**). This long pulse with the fluid-phase marker ensured labeling of the lysosomal endocytic pathway and the BC (11, 25). Those cells were then labeled for 1 min (Fig. 2, A–F) or for 10 min (Fig. 2, G–O) with Alexa 488-HDL and chased for different times. Immediately after the short labeling pulse of 1 min, Alexa 488-HDL stained almost exclusively the basolateral membrane (Fig. 2, A–C). Some endocytic vesicles were found that showed no overlap with late endosomes and lysosomes labeled with rhodamine-dextran. At the position of the BC between two neighboring cells (indicated by 1 and 2), there is a gap in the fluorescence of Alexa 488-HDL (Fig. 2, A–C, arrows). This indicates that fluorescent HDL binds to the basolateral and contiguous membrane domains but has no direct access to the BC. After a 1 min pulse and a 10 min chase, Alexa 488-HDL became enriched in the subapical region of polarized HepG2 cells, whereas Alexa 488-HDL did not accumulate in the BC labeled with rhodamine-dextran (arrows) (Fig. 2, D–F).

In cells labeled for 10 min at 37°C, Alexa 488-HDL did not become enriched in the BC (arrows) but started to accumulate in a SAC in polarized HepG2 cells (Fig. 2, G–I). In nonpolarized HepG2 cells, which lack the characteristic BC, Alexa 488-HDL accumulated in the perinuclear area, and rhodamine-labeled endosomes (thin arrowheads) often surrounded a central perinuclear spot labeled with Alexa 488-HDL (thick arrowheads) (Fig. 2, J–L). When

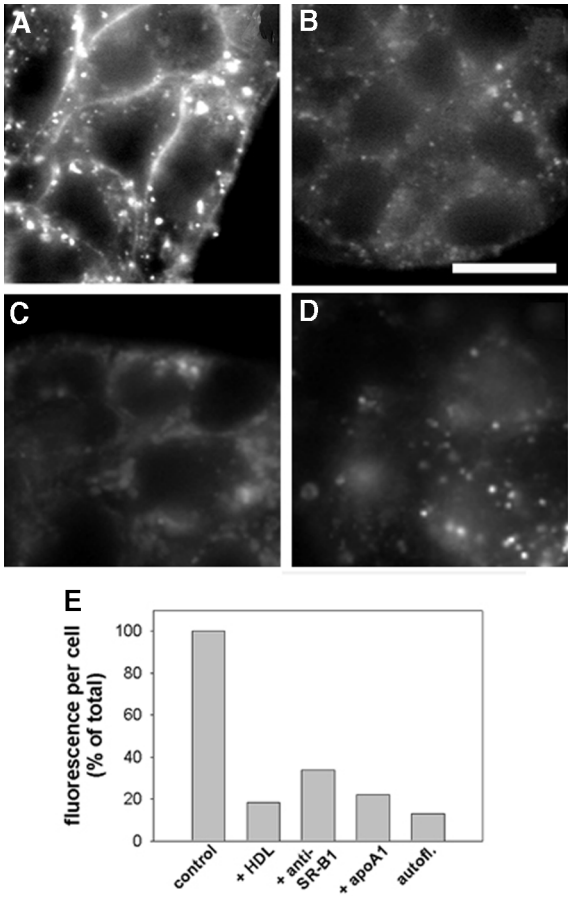

Fig. 1. Uptake of Alexa 488-labeled HDL (Alexa 488-HDL) by HepG2 cells can be blocked by nonlabeled HDL, apolipoprotein A-I (apoA-I), and antibodies against scavenger receptor class B type I (SR-BI). Cells were labeled for 2 min at 37°C with 2 μg/ml Alexa 488-HDL either in the absence (A) or presence (B) of 80 μg/ml nonlabeled HDL (40-fold excess). Cells were washed and immediately imaged on a wide-field microscope. Alternatively, cells were preincubated with an antibody against SR-BI for 5 min at 37°C before labeling with Alexa 488-HDL (C) or were labeled for 2 min at 37°C with 2 μg/ml Alexa 488-HDL in the presence of 40 μg/ml lipid-free apoA-I (D). E: Cell-associated fluorescence for control and treated cells was quantified after background subtraction and normalized to number of cells as described in Experimental Procedures. For comparison, the autofluorescence (autofl.) of cells in the green channel of the microscope was quantified. Data represent the mean of at least two experiments carried out in duplicate. Bar = 20 μm.

cells were chased for prolonged times, some Alexa 488-HDL was found in the BC (arrows) in polarized HepG2 cells (Fig. 2, M–O). Moreover, after 30 min and 60 min chases, endosomes containing Alexa 488-HDL as well as rhodamine-dextran were found near the BC (Fig. 2, M–O, thin arrowheads). The cell-associated fluorescence of Alexa 488-HDL was greatly reduced at these time points compared with the initial labeling intensity (see below). These results suggest that most initially bound Alexa 488-HDL was released from the cells at the basolateral membrane but that some Alexa 488-HDL was transported to the BC and to late endosomes and lysosomes after prolonged chase periods at 37°C.

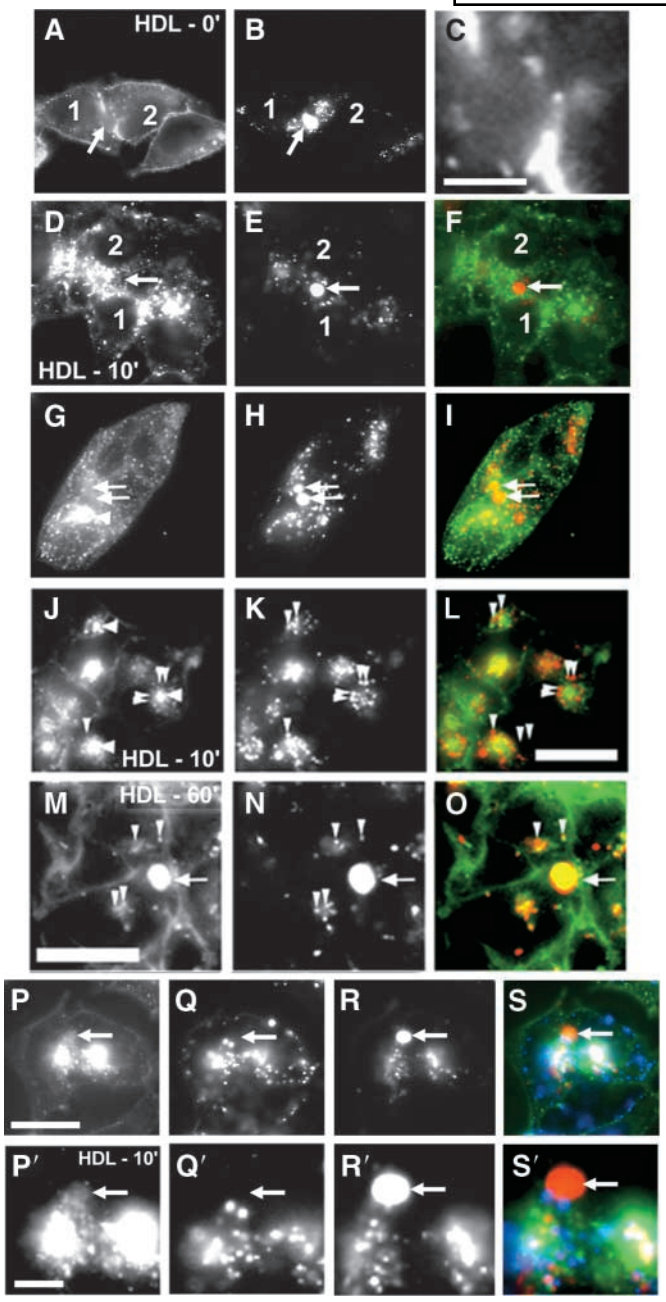

Fig. 2. Pulse-chase experiments reveal intracellular transport modes of Alexa 488-HDL. A–O: HepG2 cells were labeled with rhodamine-dextran (B, E, H, K, and N) for 1 h at 37°C. Cells were washed and labeled for either 1 min (A–F) or 10 min (G–O) with 2 μg/ml Alexa 488-HDL (A, C, D, G, J, and M), washed, and chased for 0 min (A–C), 10 min (D–L), or 60 min (M–O) at 37°C. Alexa 488-HDL initially labeled exclusively the basolateral membrane (A and C) and became internalized in endosomes (punctate fluorescence; A and D). It accumulated in a compartment underneath the biliary canaliculus (BC) (arrows) in polarized cells (D–I) and in a perinuclear compartment (thick arrowheads) in nonpolarized HepG2 cells (J–L). Alexa 488-HDL did not label the BC, which was identified by the fluorescence of rhodamine-dextran (B, E, and H) after 0 min and only very lightly after a 10 min chase. Absence of labeling after no chase was verified from the enlarged region of A showing a gap in fluorescence for Alexa 488-HDL at the position of the BC (C). Alexa 488-HDL did not colocalize with late endosomes or lysosomes containing rhodamine-dextran (thin arrowheads) (J–L). In contrast, after a 60 min chase, some Alexa 488-HDL accumulated in the BC as well as in late endosomes and lysosomes underneath the BC containing rhodamine-dextran. Cells prelabeled with rhodamine-dextran (R and R′) were incubated with Alexa 633-labeled asialo-orosomucoid (Alexa 633-ASOR; Q and Q′) for 25 min, washed, labeled with Alexa 488-HDL (P and P′) for 10 min, and chased for 10 min at 37°C (P–S′). Alexa 633-ASOR labeled late endosomes but not the BC (arrows), allowing one to distinguish BC (stained with rhodamine-dextran) from late endosomes and lysosomes labeled with either Alexa 633-ASOR or rhodamine-dextran (see above). The color overlay (F, I, L, and O) shows Alexa 488-HDL in green and rhodamine-dextran in red. The color overlay in triple-labeled cells (S and S′) shows additionally Alexa 633-ASOR in blue. Colocalization appears yellow to orange. Bars = 20 μm except in C and P′–S′, where bars = 5 μm.

To verify that the large rhodamine-dextran-labeled structures between adjacent cells were BC and not endosomes, we also labeled cells with Alexa 633-ASOR, which enters HepG2 cells by receptor-mediated endocytosis (26, 27). The kinetics of transport and intracellular itineraries of ASOR have been measured previously in polarized or nonpolarized HepG2 cells (12, 26). Here, we show that Alexa 633-ASOR enters endosomes in cells chased for 25 min with the probe, but the large intercellular structure labeled with rhodamine-dextran does not contain fluorescent ASOR (Fig. 2, P–S, arrows). This confirms our previous observations that these intercellular structures behave in many ways like BC (11, 12).

In those cells labeled and chased for 10 min each at 37°C with Alexa 488-HDL, the probe did not colocalize with Alexa 633-ASOR either in the basolateral or in the subapical region (Fig. 2, P–S). We did not find a strong overlap between Alexa 633-ASOR and rhodamine-dextran either. However, in an independent experiment in which cells were labeled with both lysosomal markers for 1 h at 37°C, we found an almost perfect overlap of Alexa 633-ASOR and rhodamine-dextran in endosomes but not in the BC (only rhodamine-dextran), allowing for clear distinguishing of both compartments (data not shown). Previous experiments in HepG2 cells incubated with ^{125}I-labeled HDL have shown that ~45% of bound HDL gets internalized within 15 min of incubation (28). Only ~27% of the internalized HDL was found to be soluble in trichloroacetic acid after a 30 min chase at 37°C (8). Thus, less than 15% of the initial cell-associated HDL is degraded in hepatic cells, which is in agreement with other work (28). This ensures that in our studies, most Alexa 488 fluorophore is on an intact protein. However, we cannot rule out that some of the fluorescence seen at later times is no longer associated with intact protein.

Alexa 488-HDL colocalizes with Tf along the endocytic pathway and accumulates in a SAC/ARC

We wanted to identify the compartments that fluorescent HDL is transported through in polarized HepG2 cells. Cells were double labeled with Alexa 488-HDL and Alexa 546-Tf for 1 min at 37°C, chased for different times, and lightly fixed with PFA. Immediately after labeling, most Alexa 488-HDL and Alexa 546-Tf localize to the basolateral membrane, and a few endocytic vesicles contain-

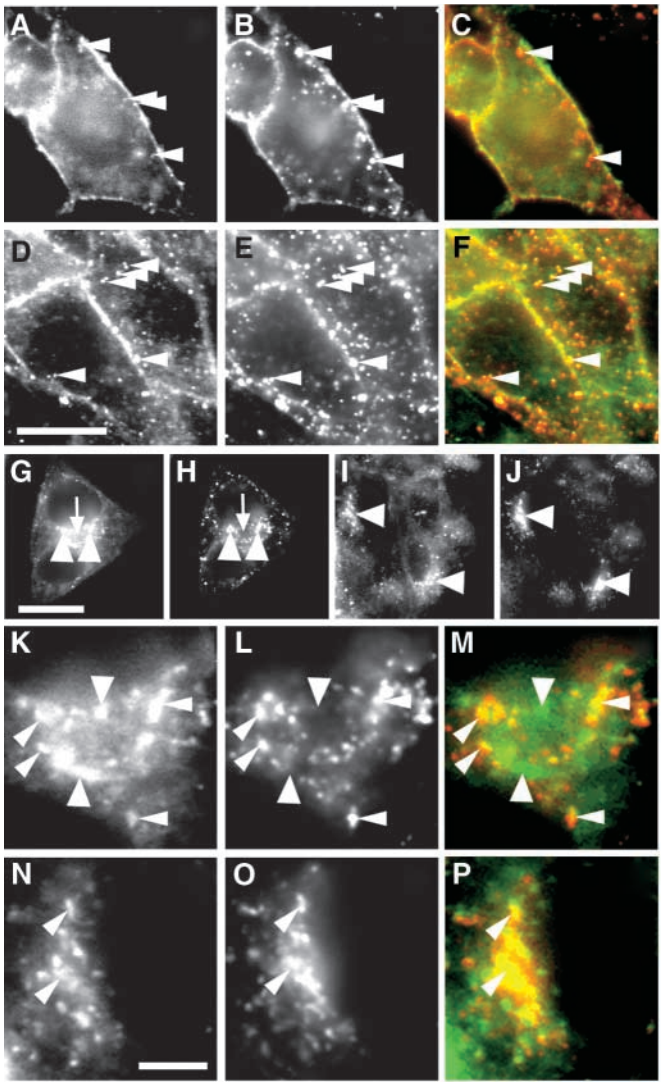

Fig. 3. Colocalization of Alexa 488-HDL with fluorescent transferrin (Tf) in the endocytic pathway. Cells were pulse-labeled with Alexa 488-HDL (A, D, G, I, K, and N) and Alexa 546-Tf (B, E, H, J, L, and O) for 1 min at 37°C. Cells were chased for 0 min (A–C), 1 min (D–F), or 10 min (G–P) at 37°C, placed on ice, and rinsed three times with ice-cold medium 1. Cells were fixed with 2% paraformaldehyde for 10 min on ice and imaged on a wide-field microscope. Immediately after pulse-labeling, most Alexa 488-HDL resided in the plasma membrane, but some endocytic vesicles containing Alexa 546-Tf were observed adjacent to the plasma membrane (A–C, arrowheads). After a 1 min chase, endocytic vesicles containing Alexa 488-HDL and Alexa 546-Tf formed in the periphery of the cells (D–F, arrowheads). After a 10 min chase, both probes accumulated in a subapical region (G and H) and in a perinuclear area (I and J) in polarized and nonpolarized cells, respectively. Only a faint staining of Alexa 488-HDL and no Alexa 546-Tf was found in the BC (arrows in G and H, enlarged in K and L). The enlarged regions of G and H (K–M) and I and J (N–P) show that Alexa 488-HDL and Alexa 546-Tf colocalize in some vesicles underneath the BC in polarized cells (K–M) and in most vesicles in nonpolarized cells (N–P) (thin arrowheads). In polarized HepG2 cells also, vesicles containing only Alexa 488-HDL were found (thick arrowheads). The color overlay (C, F, M, and P) shows Alexa 488-HDL in green and Alexa 546-Tf in red, and colocalization appears yellow. Bars = 20 μm in A–J and 5 μm in K–P.

ing both analogs were already found (**Fig. 3,** A–C). The number of double-labeled vesicles increased after a 1 min chase (Fig. 3, D–F), and after a 10 min chase, both probes became enriched in a SAC in polarized cells (Fig. 3G, H). No Alexa 546-Tf was found in the BC, whereas Alexa 488-HDL showed a faint staining of the BC compartment at this time point (Fig. 3, K–M). Because Tf is delivered to the SAC/ARC in polarized HepG2 cells (12), these data indicate that Alexa 488-HDL also accumulates in this recycling compartment after 10 min of chase at 37°C. In nonpolarized cells, Alexa 488-HDL colocalized with Alexa 546-Tf in vesicles of a juxtanuclear compartment (Fig. 3I, J, N–P, arrowheads). Comparison of label distribution in the subapical and juxtanuclear area of polarized and nonpolarized cells, respectively, shows that there are single-labeled as well as double-labeled vesicles in both types of cells. Especially in polarized HepG2 cells, Alexa 488-HDL was found in vesicles located in the SAC/ARC region, which did not contain Alexa 546-Tf (Fig. 3, K–M, thick arrowheads). This indicates the heterogeneity of organelles in the subapical region of polarized hepatic cells (12, 29, 30).

Quantitative assessment of the transport of Alexa 488-HDL in polarized HepG2 cells

We next quantified the fluorescence of Alexa 488-HDL for both labeling protocols (i.e., 1 min and 10 min pulses at 37°C) in those compartments that were found to contain Alexa 488-HDL at different time points. In cells pulse-labeled for 1 min at 37°C, Alexa 488-HDL was found to accumulate in the SAC/ARC with a fluorescence maximum at 10 min of chase (**Fig. 4A**, closed circles). Fluorescence of Alexa 488-HDL in the BC was maximal after 30 min of chase (Fig. 4A, open circles). Total cell-associated fluorescence of Alexa 488-HDL decreased during the 30 min chase (Fig. 4B). A monoexponential fit to the fluorescence decay (Fig. 4B, line) shows that the loss of cell-associated fluorescence of Alexa 488-HDL occurs with an estimated half-time of 6.9 min and an asymptote of 46%.

In cells labeled for 10 min at 37°C with Alexa 488-HDL, the initial fluorescence of Alexa 488-HDL in the SAC/ARC was higher than that in cells pulse-labeled for 1 min, and the fluorescence of Alexa 488-HDL in this compartment decreased slightly during the chase (Fig. 4C, closed circles). These observations are consistent with the maximal accumulation of Alexa 488-HDL in the SAC/ARC after a 10 min chase observed in cells labeled for 1 min with the probe (compare Fig. 4A). These data show that most Alexa 488-HDL is exported from the SAC/ARC at later time points. As the fluorescence of Alexa 488-HDL in the SAC/ARC decreased, fluorescence intensity in the BC increased in cells labeled for 10 min with Alexa 488-HDL (Fig. 4C, open circles). Total cell-associated fluorescence of Alexa 488-HDL in cells labeled for 10 min at 37°C decreased rapidly (data not shown).

It is possible that Alexa 488-HDL could be degraded and the dye released from cells (31), and this could account for the decrease of total cell-associated fluores-

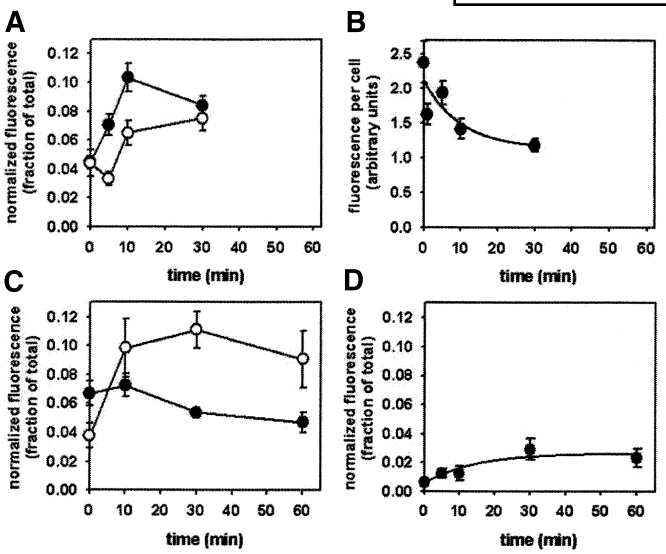

Fig. 4. Quantification of the transport kinetics of Alexa 488-HDL in polarized HepG2 cells. Cells were labeled with rhodamine-dextran for 1 h at 37°C, washed, and labeled for 1 min (A, B, and D) or 10 min (C) with 2 μg/ml Alexa 488-HDL, washed, and chased for various times. A and C: Fluorescence of Alexa 488-HDL was quantified for the subapical vesicle pool (closed symbols) and for the BC (open symbols) as described in Experimental Procedures. B: Total cell-associated fluorescence of Alexa 488-HDL was quantified in polarized HepG2 cells, which were labeled with the probe for 1 min at 37°C and chased for different times. Cell-associated fluorescence of Alexa 488-HDL could be fitted by a monoexponential decay (line in B) with $k = 0.1$ min^{-1} corresponding to a half-time of fluorescence decay of 6.9 min. D: Fluorescence of Alexa 488-HDL in late endosomes and lysosomes containing rhodamine-dextran was quantified and normalized to total cell-associated fluorescence of Alexa 488-HDL at 37°C as described in Experimental Procedures. Accumulation of Alexa 488-HDL in the lysosomal compartments could be fitted by a monoexponential function (line in D) with $k = 0.071$ min^{-1} corresponding to a half-time of 9.7 min. Data represent means ± SEM of 6–14 measurements derived from independent experiments.

cence of Alexa 488-HDL. Such a process would require the efficient transport of Alexa 488-HDL to late endosomes and lysosomes, where degradation could take place (25, 31). According to this scenario, enrichment of Alexa 488-HDL in late endosomes and lysosomes would have to be rapid to explain the rapid decrease of cell-associated fluorescence. To test this hypothesis, we measured the fluorescence of Alexa 488-HDL in endosomes that had been labeled with rhodamine-dextran. As shown in Fig. 4D, only ~2% of total cellular fluorescence of Alexa 488-HDL accumulated in late endosomes and lysosomes labeled with rhodamine-dextran during the experiment. The extent and kinetics of transport of Alexa 488-HDL to late endosomes and lysosomes, therefore, are not in accordance with the possibility of extensive degradation of Alexa 488-HDL in lysosomal compartments.

DHE incorporated into HDL is rapidly transported to the BC by an ATP-independent mechanism

HDL particles contain nonesterified cholesterol as well as cholesteryl esters. It has been shown that unesterified sterol derived from HDL is rapidly delivered to the bile of HDL-perfused rats (3, 32). Using the naturally fluorescent sterol, DHE, incorporated into Alexa 488-HDL, we studied the intracellular transport of HDL-derived sterol in polarized HepG2 cells. Cells were prelabeled with rhodamine-dextran to visualize BC, washed, and incubated for 1 min at 37°C with DHE/Alexa 488-HDL. As shown in **Fig. 5**, A–C, DHE (but not Alexa 488-HDL) became enriched in the BC after this short labeling pulse. If cells were depleted of ATP by preincubation in medium 2 containing sodium azide and deoxyglucose, uptake of Alexa 488-HDL (Fig. 5E) and Alexa 546-Tf (data not shown) was completely blocked (11). However, in these ATP-depleted cells, DHE derived from HDL continued to be delivered to the canalicular membrane (Fig. 5D). Under these conditions, staining of the basolateral membrane with DHE was higher than in control cells, in parallel with the labeling by Alexa 488-HDL in this membrane domain (Fig. 5E; see

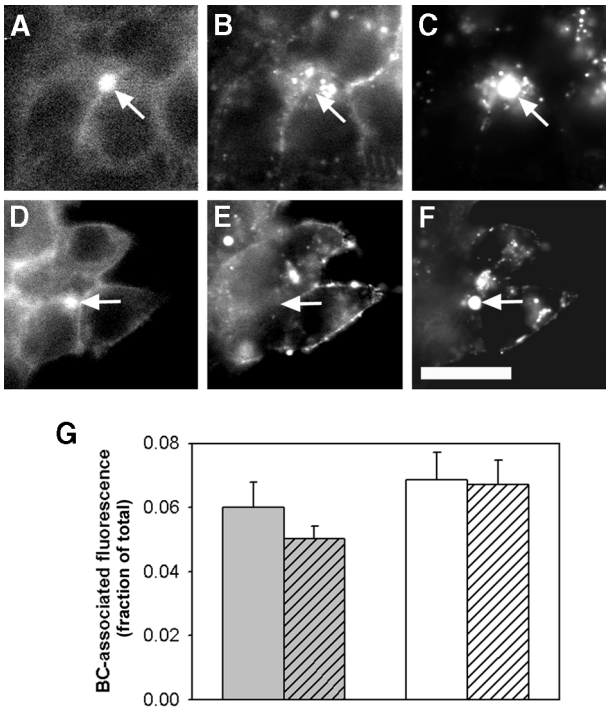

Fig. 5. Transport of dehydroergosterol (DHE) derived from Alexa 488-HDL in control and ATP-depleted HepG2 cells. Cells were first labeled with rhodamine-dextran (C and F) for 1 h at 37°C. Cells were washed and incubated for 30 min at 37°C in medium 1 (A–C, control cells) or in ATP-depletion medium (D–F, ATP-depleted cells). Cells were labeled for 1 min with Alexa 488-HDL containing DHE (DHE/Alexa 488-HDL) at 37°C, washed, and imaged. In control and ATP-depleted cells, DHE (A and D) but not Alexa 488-HDL (B and E) accumulated in the BC identified by rhodamine-dextran fluorescence (arrows). Bar = 20 μm. G: BC-associated fluorescence of DHE in control cells (gray bars) and ATP-depleted cells (gray hatched bars) was quantified for cells labeled for 1 min with DHE/Alexa 488-HDL. For comparison, cells were labeled for 1 min at 37°C with DHE loaded on methyl-β-cyclodextrin (DHE/MβCD), washed, and imaged. BC-associated fluorescence of those labeled control cells (white bars) and ATP-depleted cells (white hatched bars) was quantified. Data represent means ± SEM of 7–10 measurements derived from independent experiments.

below). In ATP-depleted cells double labeled with Alexa 546-Tf and with Alexa 488-HDL and imaged by acquisition of z-stacks, no intracellular fluorescence of either probe could be detected, in contrast to control cells. When ATP-depleted cells labeled with Alexa 546-Tf were treated with a mild acid wash, all fluorescence of Alexa 546-Tf could be removed (data not shown), confirming that internalization was blocked.

Previously, we found that DHE inserted into the plasma membrane of HepG2 cells by transfer from DHE/MβCD gets delivered rapidly to the canalicular membrane of HepG2 cells in an ATP-independent manner (11). From this result, we concluded that transport of sterol between the plasma membrane domains of hepatic cells is mostly by a nonvesicular pathway. We next compared the BC-associated fluorescence of DHE derived from HDL with that of DHE derived from MβCD (Fig. 5G). BC-associated fluorescence of DHE derived from HDL in control cells (6.0 ± 0.8%) and ATP-depleted cells (5.0 ± 0.4%) was comparable to that of DHE derived from MβCD in control cells (6.9 ± 0.9%) and ATP-depleted cells (6.7 ± 0.7%) expressed as a percentage of total cellular fluorescence of DHE. Under both conditions (i.e., in cells incubated with DHE/Alexa 488-HDL or with DHE/MβCD), ATP depletion only slightly reduced canalicular enrichment of DHE (Fig. 5G, hatched bars). This further supports the idea that DHE derived from HDL, like DHE derived from MβCD, accumulates in the BC by rapid nonvesicular transport. Interestingly, we found that the cell-associated fluorescence of DHE in ATP-depleted cells after a 1 min pulse with DHE/Alexa 488-HDL was ~4.5-fold higher than that observed in control cells (average of 10 cell couplets per condition; repeated in three separate experiments). From this observation, the following can be concluded: *i*) transfer of sterol from HDL to HepG2 cells is rapid and ATP-independent and can occur at the cell surface; and *ii*) energy depletion increases the amount of sterol transferred to hepatic cells during a brief incubation.

To estimate the quantitative contribution of nonvesicular ATP-independent transport to sterol enrichment in the BC at later time points, cells pulse-labeled with DHE/Alexa 488-HDL were chased for 10 min at 37°C. In those cells, canalicular fluorescence of DHE increased by only 10% (6.65 ± 0.7% BC-associated fluorescence expressed as a percentage of total cellular fluorescence of DHE) compared with cells without chase (**Fig. 6A**, B; compare Fig. 5G). Alexa 488-HDL was highly enriched in the SAC/ARC region in those cells, whereas fluorescence of DHE in this area was diffuse without clear vesicular enrichment. After 60 min of chase, some DHE colocalized with Alexa 488-HDL in the perinuclear or subapical region (Fig. 6C, D). Moreover, Alexa 488-HDL was found in late endosomes and lysosomes containing rhodamine-dextran (compare Fig. 2, M–O). Those endosomes did not contain DHE (Fig. 6, C′–E′). It is concluded that internalized HDL does not shuttle any DHE to degradative compartments.

The low fluorescence of DHE in the SAC/ARC region after a 10 min chase might be attributable to limited optical resolution for the weakly fluorescent DHE (11). However, quantification of the accumulation of DHE derived from the basolateral membrane by staining cells with DHE/MβCD in the SAC/ARC reveals clear differences from the transport of Alexa 488-HDL to this compartment (Fig. 6F). Whereas maximal enrichment of DHE in this compartment was not found before 30 min (a half-time could be estimated to be ~8 min), fluorescence of Alexa 488-HDL in the SAC/ARC showed a maximum after a 10 min chase (compare Fig. 4). This is in full accordance with the 10 min chase experiment for DHE (Fig. 6A, B). We conclude that vesicular cotransport of DHE bound to HDL accounts for less than 10% of the canalicular enrichment of this sterol in HepG2 cells.

To determine whether the DHE bound to HDL was transferred to HepG2 cells as a consequence of interaction with SR-BI, we measured the DHE fluorescence transferred to cells in the presence or absence of an antibody to SR-BI (Fig. 6G, H). Similar to the blocking of HDL labeled on the protein, the transfer of DHE to the HepG2 cells was inhibited by incubation with the SR-BI antibodies. This could be inferred from the lower intensity of DHE fluorescence in cells preincubated with the SR-BI antibody. In fact, in cells incubated in the presence of the SR-BI antibody, the fluorescence of DHE was 25% of that in control cells when intensities were corrected for autofluorescence. These results clearly show that SR-BI mediates the uptake of free sterol derived from HDL by HepG2 cells.

DISCUSSION

Biliary cholesterol secretion is of high importance for overall cholesterol balance. Several studies have indicated that HDLs, but no other lipoproteins, are the source for biliary cholesterol (2, 3, 32). However, it remains unclear how HDL-derived cholesterol becomes selectively targeted to the canalicular membrane for subsequent release into the bile. Earlier studies have suggested that HDL binds to the basolateral membrane of hepatic cells, resulting in the release of lipids from the lipoprotein without uptake of the particles (6, 33). However, these studies might have missed a rapid internalization of HDL and resecretion into the medium. Indeed, in various hepatoma cell lines, including HepG2 cells, a retroendocytic pathway for HDL has been described (7, 8). Uptake of HDL was blocked by ATP depletion or by exposure to low temperature, and it was sensitive to agents interfering with endocytic recycling (8, 28). In some previous studies, recycling of HDL particles was accompanied by net transfer of radioactively labeled cholesterol from HDL to hepatic cells (8).

SR-BI is the major low-affinity binding site for HDL on hepatic cells, including HepG2 cells (33–37). It has been shown that SR-BI and its associated HDL can be internalized by hepatic cells (14). We confirmed that Alexa 488-HDL is rapidly internalized by polarized HepG2 cells. The uptake was blocked by excess unlabeled HDL and by antibodies against SR-BI (~65% inhibition), consistent with

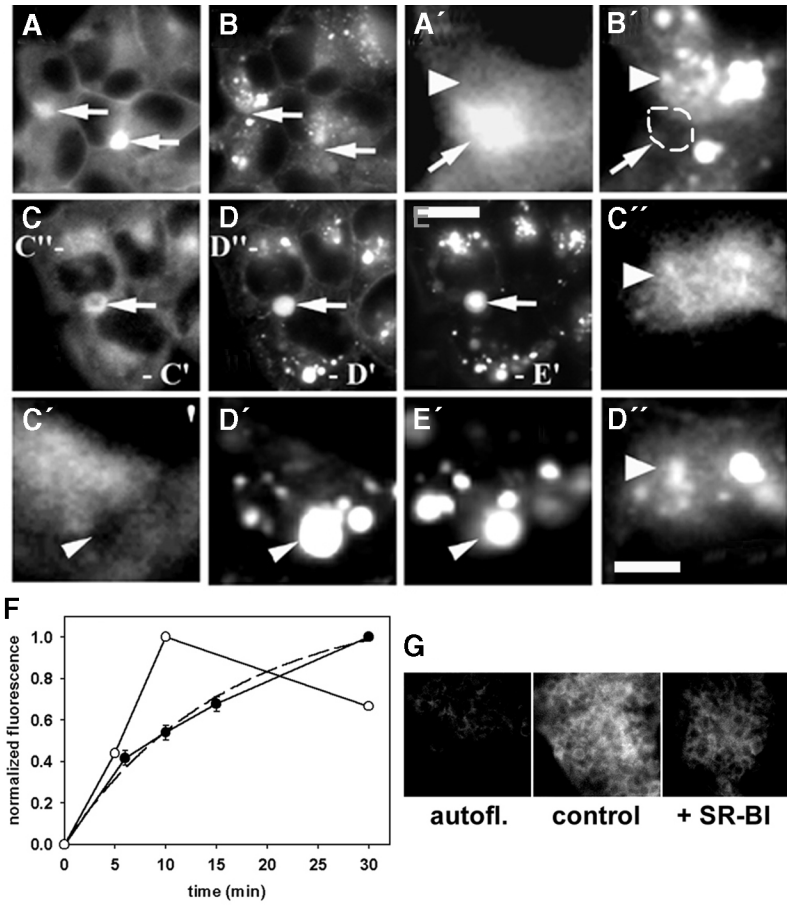

Fig. 6. Transport of DHE derived from Alexa 488-HDL after prolonged chase and inhibition of DHE uptake by SR-BI antibodies. A and B: Cells were labeled for 1 min with DHE/Alexa 488-HDL and chased for 10 min at 37°C. DHE but not Alexa 488-HDL accumulated in the BC (arrows), whereas Alexa 488-HDL but not DHE became enriched in the subapical region [arrowheads in enlarged regions, A′ and B′, outlined area corresponds to the BC seen in A′ (arrows)]. C–E: Cells were first labeled with rhodamine-dextran (E and E′) for 1 h at 37°C. Cells were washed, incubated for 1 min with DHE/Alexa 488-HDL, and chased for 60 min at 37°C. DHE (C) and Alexa 488-HDL (D) were found in the BC (arrows) labeled by rhodamine-dextran (E). Additionally, DHE became enriched in the perinuclear or subapical region, where it partially colocalized with Alexa 488-HDL (arrowheads in C′′ and D′′). Some Alexa 488-HDL was also transported to late endosomes and lysosomes labeled with rhodamine-dextran (arrowheads in D′ and E′) that lacked DHE (C′). Bars = 20 μm in A–E and 5 μm in A′–E′, C′′, and D′′. F: Quantitative comparison of the transport of DHE derived from DHE/MβCD (closed symbols) (cells were labeled for 1 min with DHE/MβCD and chased for various times) and Alexa 488-HDL (open symbols) (see Fig. 4A; normalized here to maximal intensity) to the subapical compartment/apical recycling compartment (SAC/ARC). Enrichment of DHE in the SAC/ARC could be fitted to a monoexponential function (dashed line) giving a half-time of 7.9 min. Data represent means ± SEM of eight measurements derived from independent experiments. G: HepG2 cells were preincubated with antibodies against SR-BI for 5 min at 37°C and labeled with DHE/Alexa 488-HDL for 10 min at 37°C in the presence of SR-BI antibody. autofl., autofluorescence.

uptake via SR-BI. We also found reduced uptake of Alexa 488-HDL by lipid-free apoA-I (~80% inhibition). It has been shown that apoA-I is internalized by an ectopic ATP synthase in HepG2 cells (38). However, lipid-free apoA-I can compete with ^{125}I-HDL binding to SR-BI, in accordance with our results (24). Because apoA-I is an exchangeable lipoprotein, it is theoretically possible that some Alexa 488-labeled apolipoprotein exchanges out of the HDL particle, binds to a receptor for lipid-free apoA-I, and becomes internalized. From our experiments, we cannot completely rule out that this occurs to some extent. However, because the SR-BI antibody inhibited the uptake of HDL labeled either in the protein or in the lipid (DHE) to a similar extent, we suggest that SR-BI is the major receptor for the uptake of our labeled HDL into HepG2 cells. It has been suggested that the expression of SR-BI is required for reverse cholesterol transport by mediating the selective uptake of HDL-associated lipids by the liver and their subsequent transfer to the bile (23, 32). Administration of HDL labeled with the lipid analog dioctadecanoyl-3,3,3′,3′-tetramethylindocarbocyanine perchlorate (DiI-C18) to mice overexpressing SR-BI resulted in the secretion of DiI-C18 into the bile of those animals (23). Overexpression of SR-BI in mice also resulted in acceleration of the biliary release of [^{3}H]cholesterol derived from administered HDL compared with control mice (32). This rapid sterol transport from HDL into bile led to a model in which SR-BI mediates the rapid transfer of free cholesterol to the canalicular membrane by a process that is controlled by ATP-dependent lipid translocation across the canalicular membrane (32). We have examined this process by comparing the fates of Alexa 488-HDL and DHE.

Colocalization of Alexa 488-HDL with internalized Tf was found as early as after 1 min of incubation with the probes (Fig. 3), suggesting that Alexa 488-HDL is most likely internalized together with fluorescent Tf by clathrin-dependent endocytosis. Several other studies have concluded that uptake of HDL in HepG2 cells and in enterocytes (28, 39) is clathrin-mediated, which would be consistent with our interpretation. However, a previous study found that uptake of HDL by hepatocyte couplets is not affected by the expression of dominant-inhibitory forms of dynamin, suggesting that the uptake is by a clathrin-independent mechanism (14). From our experiments, we cannot rule out the possibility that HDL is endocytosed by a separate mechanism and is then delivered rapidly into the endosomes containing Tf.

It was shown previously that SR-BI and labeled HDL colocalize with fluorescent Tf in endosomes adjacent to the BC of primary hepatocyte couplets (14). We found that after internalization, some Alexa 488-HDL was transported to recycling endosomes containing Tf located ad-

jacent to the BC of HepG2 cells. Colocalization with fluorescent Tf in this region suggests that Alexa 488-HDL is transported to a SAC/ARC, previously shown to be a major pool of sterol and recycling lipids in those cells (11, 12, 40). This suggested that the SAC/ARC might play a pivotal role in the selective transport of sterol derived from the HDL particle to the canalicular membrane. However, without a way to directly image sterols, it was not possible to determine at which point in the endocytic itinerary the pathways of the sterol and the protein diverged.

Our kinetic results presented in Figs. 3–6 help to explain the selective and rapid sorting of free sterol from HDL that has been described in previous studies: HDL binds to a receptor at the basolateral membrane (probably SR-BI) followed by rapid release of free cholesterol from the HDL particle and shuttling of this sterol to the canalicular membrane. We show here that SR-BI mediates (at least partially) the endocytosis of HDL particles by HepG2 cells as well as the uptake of HDL-associated free sterol. This is in accordance with the proposed function of SR-BI in vivo, although the underlying mechanism for this dual function of SR-BI (i.e., uptake of a lipoprotein versus release and shuttling of its free sterol content) is not known at present (14, 23, 24, 32). After delivery to the basolateral membrane, transfer of sterol from HDL to the BC could occur mainly by nonvesicular transport processes, including flipping of sterol to the cytoplasmic leaflet of the plasma membrane and lateral diffusion toward the BC (11). The previously measured half-time of transport of DHE from the basolateral to the canalicular membrane of HepG2 cells (1–2 min) is consistent with the in vivo clearance rate of cholesterol derived from HDL (1–3 min) (3, 32). This is also consistent with the observation that there is little additional delivery of DHE to the BC when the chase period is extended from 1 min to 10 min. Our comparisons of Alexa 488-HDL traffic versus DHE traffic suggest that the transport of nonesterified sterol from HDL to the canalicular membrane is too fast to be accounted for by vesicle transcytosis through hepatic cells. Moreover, this transport is largely energy-independent, whereas vesicle transport is known to require energy. We thus conclude that nonesterified sterol derived from HDL is rapidly transported to the canalicular membrane by a largely ATP-independent nonvesicular pathway, which includes rapid transbilayer migration of the sterol. Remarkably, we found a 4.5-fold increase in cell-associated DHE derived from HDL during a 1 min incubation when cells were energy depleted. At present, we do not know the basis for this increased transfer of sterol. One possible explanation could be that in normal, energy-replete cells, there is an active, energy-dependent flipping of inner leaflet sterol back to the outer leaflet to maintain overall interleaflet asymmetry. Thus, there would be less sterol in the inner leaflet at any given time, and thus, less of them will be able to access the nonvesicular cytosolic carriers for transport to the canalicular membrane. Sterol in the outer leaflet also could be accessible for acceptor-mediated efflux from cells. Indeed, an ATP-dependent transport step has been suggested for cholesterol efflux to lipid-free apoA-I in various cell types.

Recently, it has been shown that the ABC half-transporters ABCG8 and ABCG5 dimerize at the canalicular membrane of polarized WIF-B cells and mediate the biliary secretion of cholesterol but not phospholipids in mice overexpressing the proteins (4, 5). Thus, an ATP-dependent process results in cholesterol release from the membrane and incorporation into PC-bile salt micelles or vesicles in the canalicular lumen (41). The energy-dependent step might involve an export pump that facilitates cholesterol transport to the luminal leaflet of the canalicular membrane or a process that increases the efficiency of cholesterol transfer to acceptors in the bile. This energy-requiring process would occur after the ATP-independent delivery of sterol to the canalicular membrane.

Although free sterol derived from HDL is mainly delivered to the canalicular membrane by nonvesicular transport, most of the internalized HDL is returned to the plasma membrane and released. One pathway would involve return from the SAC/ARC back to the basolateral plasma membrane. The measured half-time for the release of HDL from HepG2 cells (6.9 min) is faster than most recycling from ERCs (25). However, there are faster, more direct recycling pathways from early sorting endosomes (42, 43), and such a pathway may be operating in polarized HepG2 cells, ensuring the efficient resecretion of internalized HDL into the culture medium. Because cholesterol would be removed rapidly from the cell-associated HDL, the resecreted particles would have altered lipid compositions, as has been observed experimentally (14).

Our results suggest that HDL is internalized by HepG2 cells, but this internalization is apparently not required for the transport of free cholesterol to the canalicular membrane. In contrast, internalization of HDL into the SAC/ARC might be important for the uptake and selective transcytosis of cholesterol esters (14). Further studies with DHE esters incorporated into HDL may help to understand the transcytosis of these esters.

The authors thank Andreas Herrmann (Department of Molecular Biophysics, Humboldt University, Berlin, Germany) for critical reading of the manuscript and are grateful to David L. Silver, Alan Tall, and Ira Tabas (Columbia University, New York, NY) for kindly providing human HDL_3 and antibodies against SR-BI. Allan Wolkoff and Richard Stockert (Albert Einstein College of Medicine, New York, NY) are acknowledged for providing ASOR. This work was supported by grants from the National Institutes of Health (DK-27083) and the Ara Parseghian Medical Research Foundation (F.R.M.). D.W. was supported by a Postdoctoral Fellowship for Biomedical Research from the Charles Revson Foundation.

REFERENCES

1. Kuipers, F., R. P. J. Oude Elferink, H. Verkade, and A. K. Groen. 1997. Mechanisms and (patho)physiological significance of biliary cholesterol secretion. *Subcell. Biochem.* **28:** 1053–1060.

2. Robins, S. J., and J. M. Fasulo. 1997. High density lipoproteins, but not other lipoproteins, provide a vehicle for sterol transport to bile. *J. Clin. Invest.* **99:** 380–384.
3. Robins, S. J., and J. M. Fasulo. 1999. Delineation of a novel hepatic route for the selective transfer of unesterified sterols from high-density lipoproteins to bile: studies using the perfused rat liver. *Hepatology.* **29:** 1541–1548.
4. Yu, L., J. Li-Hawkins, R. E. Hammer, K. E. Berge, J. D. Horton, J. C. Cohen, and H. H. Hobbs. 2002. Overexpression of ABCG5 and ABCG8 promotes biliary cholesterol secretion and reduces fractional absorption of dietary cholesterol. *J. Clin. Invest.* **110:** 671–680.
5. Graf, G. A., W. P. Li, R. D. Gerard, I. Gelissen, A. White, J. C. Cohen, and H. H. Hobbs. 2002. Coexpression of ATP-binding cassette proteins ABCG5 and ABCG8 permits their transport to the apical surface. *J. Clin. Invest.* **110:** 659–669.
6. Jackle, S., F. Rinninger, T. Lorenzen, H. Greten, and E. Windler. 1993. Dissection of compartments in rat hepatocytes involved in the intracellular trafficking of high-density lipoprotein particles or their selectively internalized cholesteryl esters. *Hepatology.* **17:** 455–465.
7. Kambouris, A. M., P. D. Roach, G. D. Calvert, and P. J. Nestel. 1990. Retroendocytosis of high density lipoproteins by the human hepatoma cell line, HepG2. *Arteriosclerosis.* **10:** 582–590.
8. DeLamatre, J. G., T. G. Sarphie, R. C. Archibold, and C. A. Hornick. 1990. Metabolism of apoE-free high density lipoprotein in rat hepatoma cells: evidence for a retroendocytic pathway. *J. Lipid Res.* **31:** 191–202.
9. Silver, D. L., N. Wang, and A. R. Tall. 2000. Defective HDL particle uptake in ob/ob hepatocytes causes decreased recycling, degradation, and selective lipid uptake. *J. Clin. Invest.* **105:** 151–159.
10. Sormunen, R., S. Eskelinen, and V. P. Lehto. 1993. Bile canaliculus formation in cultured HepG2 cells. *Lab. Invest.* **68:** 652–662.
11. Wüstner, D., A. Herrmann, M. Hao, and F. R. Maxfield. 2002. Rapid nonvesicular transport of sterol between the plasma membrane domains of polarized hepatic cells. *J. Biol. Chem.* **277:** 30325–30336.
12. Wüstner, D., S. Mukherjee, F. R. Maxfield, P. Müller, and A. Herrmann. 2001. Vesicular and nonvesicular transport of phosphatidylcholine in polarized HepG2 cells. *Traffic.* **2:** 277–296.
13. Yamashiro, D. J., B. Tycko, S. R. Fluss, and F. R. Maxfield. 1984. Segregation of transferrin to a mildly acidic (pH 6.5) para-Golgi compartment in the recycling pathway. *Cell.* **37:** 789–800.
14. Silver, D. L., N. Wang, X. Xiao, and A. R. Tall. 2001. High density lipoprotein (HDL) particle uptake mediated by scavenger receptor class B type 1 results in selective sorting of HDL cholesterol from protein and polarized cholesterol secretion. *J. Biol. Chem.* **276:** 25287–25293.
15. Hao, M., S. X. Lin, O. J. Karylowski, D. Wüstner, T. E. McGraw, and F. R. Maxfield. 2002. Vesicular and non-vesicular sterol transport in living cells. The endocytic recycling compartment is a major sterol storage organelle. *J. Biol. Chem.* **277:** 609–617.
16. Sheets, E. D., D. Holowka, and B. Baird. 1999. Critical role for cholesterol in Lyn-mediated tyrosine phosphorylation of FcepsilonRI and their association with detergent-resistant membranes. *J. Cell Biol.* **145:** 877–887.
17. Loura, L. M., and M. Prieto. 1997. Dehydroergosterol structural organization in aqueous medium and in a model system of membranes. *Biophys. J.* **72:** 2226–2236.
18. Mukherjee, S., X. Zha, I. Tabas, and F. R. Maxfield. 1998. Cholesterol distribution in living cells: fluorescence imaging using dehydroergosterol as a fluorescent cholesterol analog. *Biophys. J.* **75:** 1915–1925.
19. Ghosh, R. N., and F. R. Maxfield. 1995. Evidence for nonvectorial, retrograde transferrin trafficking in the early endosomes of HEp2 cells. *J. Cell Biol.* **128:** 549–561.
20. Mukherjee, S., T. T. Soe, and F. R. Maxfield. 1999. Endocytic sorting of lipid analogues differing solely in the chemistry of their hydrophobic tails. *J. Cell Biol.* **144:** 1271–1284.
21. Mayor, S., J. F. Presley, and F. R. Maxfield. 1993. Sorting of membrane components from endosomes and subsequent recycling to the cell surface occurs by a bulk flow process. *J. Cell Biol.* **121:** 1257–1269.
22. Mallet, W. G., and F. R. Maxfield. 1999. Chimeric forms of furin and TGN38 are transported from the plasma membrane to the trans-Golgi network via distinct endosomal pathways. *J. Cell Biol.* **146:** 345–359.
23. Kozarsky, K. F., M. H. Donahee, A. Rigotti, S. N. Iqbal, E. R. Edelman, and M. Krieger. 1997. Overexpression of the HDL receptor SR-BI alters plasma HDL and bile cholesterol levels. *Nature.* **387:** 414–417.
24. Thuahnai, S. T., S. Lund-Katz, G. M. Anantharamaiah, D. L. Williams, and M. C. Phillips. 2003. A quantitative analysis of apolipoprotein binding to SR-BI: multiple binding sites for lipid-free and lipid-associated apolipoproteins. *J. Lipid Res.* **44:** 1132–1142.
25. Mukherjee, S., R. N. Ghosh, and F. R. Maxfield. 1997. Endocytosis. *Physiol. Rev.* **77:** 759–803.
26. Tycko, B., C. H. Keith, and F. R. Maxfield. 1983. Rapid acidification of endocytic vesicles containing asialoglycoprotein in cells of a human hepatoma line. *J. Cell Biol.* **97:** 1762–1776.
27. Stoorvogel, W., H. J. Geuze, and G. J. Strous. 1987. Sorting of endocytosed transferrin and asialoglycoprotein occurs immediately after internalization in HepG2 cells. *J. Cell Biol.* **104:** 1261–1268.
28. Garcia, A., R. Barbaras, X. Collet, A. Bogyo, H. Chap, and B. Perret. 1996. High-density lipoprotein 3 receptor-dependent endocytosis pathway in a human hepatoma cell line (HepG2). *Biochemistry.* **35:** 13064–13071.
29. van Ijzendoorn, S. C., and D. Hoekstra. 1999. Polarized sphingolipid transport from the subapical compartment: evidence for distinct sphingolipid domains. *Mol. Biol. Cell.* **10:** 3449–3461.
30. Maier, O., and D. Hoekstra. 2003. Trans-Golgi network and subapical compartment of HepG2 cells display different properties in sorting and exiting of sphingolipids. *J. Biol. Chem.* **278:** 164–173.
31. Paresce, D. M., H. Chung, and F. R. Maxfield. 1997. Slow degradation of aggregates of the Alzheimer's disease amyloid beta-protein by microglial cells. *J. Biol. Chem.* **272:** 29390–29397.
32. Ji, Y., N. Wang, R. Ramakrishnan, E. Sehayek, D. Huszar, J. L. Breslow, and A. R. Tall. 1999. Hepatic scavenger receptor BI promotes rapid clearance of high density lipoprotein free cholesterol and its transport into bile. *J. Biol. Chem.* **274:** 33398–33402.
33. Rinninger, F., M. Brundert, S. Jackle, P. R. Galle, C. Busch, J. R. Izbicki, X. Rogiers, D. Henne-Bruns, B. Kremer, C. E. Broelsch, and H. Greeten. 1994. Selective uptake of high-density lipoprotein-associated cholesteryl esters by human hepatocytes in primary culture. *Hepatology.* **19:** 1100–1114.
34. Martinez, L. O., V. Georgeaud, C. Rolland, X. Collet, F. Terce, B. Perret, and R. Barbaras. 2000. Characterization of two high-density lipoprotein binding sites on porcine hepatocyte plasma membranes: contribution of scavenger receptor class B type I (SR-BI) to the low-affinity component. *Biochemistry.* **39:** 1076–1082.
35. Witt, W., I. Kolleck, H. Fechner, P. Sinha, and B. Rüstow. 2000. Regulation by vitamin E of the scavenger receptor BI in rat liver and HepG2 cells. *J. Lipid Res.* **41:** 2009–2016.
36. Barbaras, R., X. Collet, H. Chap, and B. Perret. 1994. Specific binding of free apolipoprotein A-I to a high-affinity binding site on HepG2 cells: characterization of two high-density lipoprotein sites. *Biochemistry.* **33:** 2335–2340.
37. Georgeaud, V., A. Garcia, D. Cachot, C. Rolland, F. Terce, H. Chap, X. Collet, B. Perret, and R. Barbaras. 2000. Identification of an ApoA-I ligand domain that interacts with high-affinity binding sites on HepG2 cells. *Biochem. Biophys. Res. Commun.* **267:** 541–545.
38. Martinez, L. O., S. Jacquet, J-P. Esteve, C. Rolland, E. Cabezon, E. Champagne, T. Pineau, V. Georgeaud, J. E. Walker, F. Terce, X. Collet, B. Perret, and R. Barbaras. 2003. Ectopic beta-chain of ATP synthase is an apolipoprotein A-I receptor in hepatic HDL endocytosis. *Nature.* **421:** 75–79.
39. Rogler, G., G. Herold, C. Fahr, M. Fahr, D. Rogler, F. M. Reimann, and E. F. Stange. 1992. High-density lipoprotein 3 retroendocytosis: a new lipoprotein pathway in the enterocyte (Caco-2). *Gastroenterology.* **103:** 469–480.
40. van Ijzendoorn, S. C. D., M. M. P. Zegers, J. W. Kok, and D. Hoekstra. 1997. Segregation of glucosylceramide and sphingomyelin occurs in the apical to basolateral transcytotic route in HepG2 cells. *J. Cell Biol.* **137:** 347–357.
41. Wittenburg, H., and M. C. Carey. 2002. Biliary cholesterol secretion by the twinned sterol half-transporters ABCG5 and ABCG8. *J. Clin. Invest.* **110:** 605–609.
42. Hao, M., and F. R. Maxfield. 2000. Characterization of rapid membrane internalization and recycling. *J. Biol. Chem.* **275:** 15279–15286.
43. Sheff, D. R., E. A. Daro, M. Hull, and I. Mellman. 1999. The receptor recycling pathway contains two distinct populations of early endosomes with different sorting functions. *J. Cell Biol.* **145:** 123–139.